

# A Meshless Method for Variational Nonrigid 2-D Shape Registration

Wei Liu and Eraldo Ribeiro

Computer Vision and Bio-Inspired Computing Laboratory  
Department of Computer Sciences  
Florida Institute of Technology  
Melbourne, FL 32901, U.S.A.

**Abstract.** We present a method for nonrigid registration of 2-D geometric shapes. Our contribution is twofold. First, we extend the classic chamfer-matching energy to a variational functional. Secondly, we introduce a meshless deformation model that can adapt computation to the shape boundary. In our method, 2-D shapes are implicitly represented by a distance transform, and the registration error is defined based on the shape contours' mutual distances. Additionally, we model global shape deformation as an approximation blended from local fields using partition-of-unity. The deformation field is regularized by penalizing inconsistencies between local fields. This representation can be adaptive to the shape's contour, leading to registration that is both flexible and efficient. Finally, shape registration is achieved by minimizing a variational chamfer-energy functional combined with the consistency regularizer using an efficient quasi-Newton algorithm. We demonstrate the effectiveness of our registration method on a number of experiments.

## 1 Introduction

Registering 2-D shapes that have been deformed by nonlinear mappings is a challenging problem that has applications in many areas including medical imaging [1] and shape recognition [2]. Similarities can be drawn between shape registration and general nonrigid image-registration problems, with variational methods marking the state-of-the-art for nonrigid image registration. On the other hand, current variational shape-registration methods are sensitive to shape noise and occlusion. In this paper, we extend the work in [3, 4], and propose a robust and efficient variational shape-registration method using an implicit distance transform representation and a meshless deformation model.

Shape registration is an ill-posed problem as there can be many ambiguous solutions. Similarly to nonrigid image registration [5], the ill-posedness in shape registration methods is often addressed by regularizing solutions through statistical [6] or variational priors [3, 4]. In contrast with image registration, where texture information may be abundant, shape registration often deals with images containing very sparse signal, that can be highly sensitive to image noise.

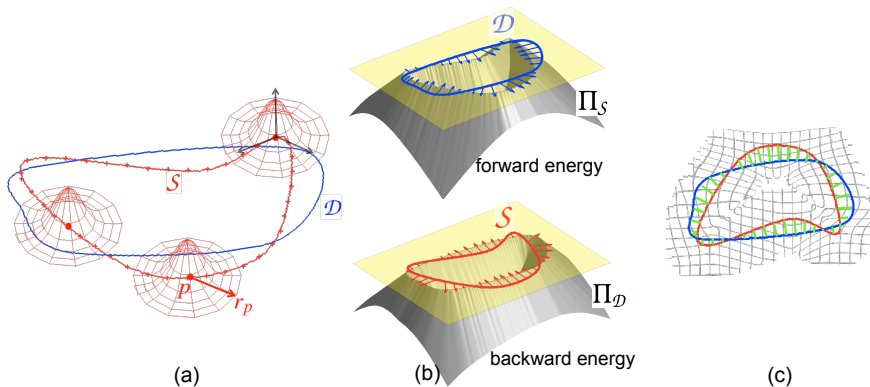


**Fig. 1.** Meshless shape registration. (a) Source (red curve) and target (blue curve) shapes. Nodes are placed along the contour. Three nodes are illustrated with their corresponding influence regions (Section 3). (b) Forward and backward registration error (Section 2). (c) Blended global deformation map and correspondence after registration.

Although statistical priors help improve robustness, these priors are often tailored to different classes of shapes, requiring a separate class-specific training stage. On the other hand, while variational methods make fewer assumptions about the shapes, these methods can be more sensitive to occlusion and noise.

Our focus in this paper is on variational shape-registration methods. In this class of methods, existing approaches differ in three main aspects [4]: shape representation, deformation model, and registration criterion. Implicit shape models can be obtained by considering a shape to be a distance-transform’s zero level set [3, 4]. Advantages of using implicit representations include fewer model parameters, and easy extension to higher dimensions. Moreover, distance functions are redundant 2-D representations of 1-D shapes, and similar distance functions lead to similar shapes. Thus, contour registration can be achieved using traditional image-registration techniques [3, 4]. Indeed, the underlining registration criterion can be simply the squared-difference of distance functions, and the deformation model can be non-parametric [3], or parametric as B-splines [4]. However, distance transforms are sensitive to shape noise, and its redundancy leads to unnecessary computation. These problems are only partially addressed [3, 4] by limiting the registration around shape contours based on a proximity function.

In this paper, we adopt an implicit shape model based on distance functions, and address some of the above problems by removing the redundancy from both the registration criterion and the deformation model. First, we modify the registration criterion by considering distance errors at shape boundaries only. This criterion can be seen as a variational form of the classic chamfer-matching functional. As in chamfer matching, the proposed functional is robust to both spurious points and shape occlusions. Secondly, we propose a mesh-free deformation model to adapt registration around shape contours. In contrast to B-spline

models that rely on a control-point grid with explicit connections, our meshless deformation model represents shape deformation by blending together local deformations using partition-of-unity [7]. These local deformations can be centered at arbitrarily distributed nodes (particles), allowing us to model shapes of different topologies, and to handle irregular shape deformations. By aligning the nodes along the shape contour, we can remove the redundancy in the registration process. Since rigid shape alignment can be done using off-the-shelf methods such as shape context [1], mutual information [4], and chamfer matching [2], we assume that shapes are aligned beforehand using a rigid transformation, and focus ourselves on the nonrigid registration part (i.e., global-to-local approach [1]).

This paper is organized as follows. In Section 2, we review the general framework for nonrigid registration using distance functions [3, 4], and then introduce our variational dissimilarity function. In Section 3, we introduce our meshless shape-deformation representation, and discuss the numerical minimization of the proposed dissimilarity functional. Section 4 shows registration results on both synthetic and real-world images.

## 2 Distance functions and nonrigid registration

The goal of shape registration is to deform a source shape onto a target shape. This is achieved by searching for the best deformation field that minimizes a dissimilarity measure between the shapes. Formally, if  $S$  and  $\mathcal{D}$  represent source and target shapes, respectively, and  $F$  is a dissimilarity measure between the two shapes, we seek for a warping field  $\mathbf{u}(\mathbf{x})$  that satisfies the following equation:

$$\arg \min_{\mathbf{x}'} F(\mathcal{D}(\mathbf{x}'), S(\mathbf{x}), \mathbf{x}'), \quad \mathbf{x}' = \mathbf{x} + \mathbf{u}(\mathbf{x}), \quad (1)$$

where  $\mathbf{x}$  is a coordinate vector. The dissimilarity measure  $F$  usually depends on the shape model. In this paper, we implicitly represent a shape  $S$  as the zero level set of its distance transform  $\Pi_S$  [3, 4], where  $S$  defines a partition of the image domain  $\Omega$ . The model is given by:

$$\Pi_S = \begin{cases} 0, & \mathbf{x} \in S \\ +D_S(\mathbf{x}) > 0, & \mathbf{x} \in R_S \\ -D_S(\mathbf{x}) < 0, & \mathbf{x} \in [\Omega - R_S] \end{cases}, \quad (2)$$

where  $D_S$  is the minimum Euclidean distance between location  $\mathbf{x}$  and shape  $S$ , and  $R_S$  is the region inside  $S$ . Here,  $F$  can be defined as the squared-sum of distance transform differences, and registration is achieved by minimizing:

$$E(\mathbf{u}) = \underbrace{\int_{\Omega} N_{\delta}(\Pi_{\mathcal{D}} - \Pi_S)^2 d\mathbf{x}}_{\text{data term}} + \alpha \underbrace{\int_{\Omega} N_{\delta}(\|\nabla \mathbf{u}_x\|^2 + \|\nabla \mathbf{u}_y\|^2) d\mathbf{x}}_{\text{smoothness regularizer}}. \quad (3)$$

In (3),  $\Pi_S$  and  $\Pi_{\mathcal{D}}$  are distance transforms of the source and target shapes, respectively. The proximity function  $N_{\delta}$  limits the data-term evaluation to be near

the shape’s boundary, and the smoothness term penalizes for spatial variations in the estimated deformation field.

The above representation facilitates the use of existing nonrigid registration techniques to solve shape registration. However, two issues need to be considered. First, although similar distance functions lead to similar shapes, similar shapes may not necessarily produce similar distance functions. For example, a spurious point located far from the shape can offset the distance transform, leading to different 2-D representations. In other words, This implicit representation’s redundancy breaks the continuity between shapes and their representation domains. This argument is supported in [3] by observing that scaling affects distance functions. In fact, a scaling factor is estimated separately in [3], and shape noise is only partially addressed in [3, 4] by using the proximity function  $N_\delta$ . Secondly, registering 2-D distance functions leads to extra computation as deformation models register the whole image plane. The use of the proximity function [3, 4] reduces these problems but the formulation becomes more complicated.

Next, we propose a dissimilarity measure by using a novel variational formulation of the chamfer-matching energy that does not use a proximity function.

## 2.1 Variational chamfer-matching energy

When the source shape  $\mathcal{S}$  is aligned with the target shape  $\mathcal{D}$ , the deformed shape  $\mathcal{S}(\mathbf{x} + \mathbf{u})$  will coincide with the zero level set of  $\Pi_{\mathcal{D}}$ , i.e.,  $\mathcal{S}(\mathbf{x} + \mathbf{u}) \Pi_{\mathcal{D}} = 0$ . Here, we represent shape  $\mathcal{S}$  by a binary contour map, and enforce alignment between shapes by minimizing the squared sum  $\int_{\Omega} |\mathcal{S}(\mathbf{x} + \mathbf{u}) \Pi_{\mathcal{D}}|^2 d\mathbf{x}$ , which corresponds to the classic chamfer-matching energy function [2]. However, this functional can be ill-posed. For example, the energy function will vanish for any deformation field that shrinks the source shape to a single point on shape  $\mathcal{D}$ . Similarly to *symmetric chamfer-matching energy* [8], we can address this problem by including a symmetric term that measures the distance-error between target and source shapes. Additionally, we compensate for scaling by dividing the distance-error by the contours’ length, and minimize the following functional:

$$E^d(\mathbf{u}) = \frac{1}{A} \left[ \underbrace{\int_{\Omega} |\mathcal{S}(\mathbf{x} + \mathbf{u}) \Pi_{\mathcal{D}}|^2 d\mathbf{x}}_{\text{forward energy } E^f} + \underbrace{\int_{\Omega} |\mathcal{D}(\mathbf{x}) \Pi_{\mathcal{S}(\mathbf{x}+\mathbf{u})}|^2 d\mathbf{x}}_{\text{backward energy } E^b} \right], \quad (4)$$

where  $A = \int_{\Omega} \mathcal{S}(\mathbf{x} + \mathbf{u}) d\mathbf{x} \int_{\Omega} \mathcal{D}(\mathbf{x}) d\mathbf{x}$  is a normalizing factor. Since  $E^d(\mathbf{u})$  is independent on the sign of  $\Pi$ , we will assume that  $\Pi_{\mathcal{S}} \geq 0$  and  $\Pi_{\mathcal{D}} \geq 0$ .

The registration error is directly measured using the shape contours without resorting to a proximity function as in [3]. As in chamfer matching, the usage of distance transform facilitates optimization by providing an energy gradient. For example, the gradient of the forward-energy term can be calculated as follows:

$$\frac{\partial E^f(\mathbf{u})}{\partial \mathbf{u}} = 2 \int_{\Omega} [\mathcal{S}(\mathbf{x} + \mathbf{u}) \Pi_{\mathcal{D}}] \Pi_{\mathcal{D}} \frac{\partial \mathcal{S}(\mathbf{x} + \mathbf{u})}{\partial \mathbf{x}} d\mathbf{x}. \quad (5)$$

Since  $s$  is a binary map, then  $\Pi_{\mathcal{D}} \frac{\partial s(\mathbf{x}+\mathbf{u})}{\partial \mathbf{x}} = \frac{\partial \Pi_{\mathcal{D}}}{\partial \mathbf{x}} s(\mathbf{x}+\mathbf{u})$  and  $s(\mathbf{x}+\mathbf{u})s(\mathbf{x}+\mathbf{u}) = s(\mathbf{x}+\mathbf{u})$ . Substituting these identities into (5), we have:

$$\frac{\partial E^f(\mathbf{u})}{\partial \mathbf{u}} = 2 \int_{\Omega} [s(\mathbf{x}+\mathbf{u}) \Pi_{\mathcal{D}}] \frac{\partial \Pi_{\mathcal{D}}}{\partial \mathbf{x}} d\mathbf{x}. \quad (6)$$

For the backward-energy term in (4), its derivative involves calculating the distance transform of the deformed source shape, i.e.,  $\Pi_{s(\mathbf{x}+\mathbf{u})}$ . Fortunately, by substituting variables, Equation 4 can be re-written as  $\int_{\Omega} |\mathcal{D}(\mathbf{x}) \Pi_{s(\mathbf{x}+\mathbf{u})}|^2 d\mathbf{x} = \int_{\Omega} |\mathcal{D}(\mathbf{x}-\mathbf{u}) \Pi_{s(\mathbf{x})}|^2 d\mathbf{x}$ , and then expanded as we did in Equation 6 to have:

$$\frac{\partial E^b}{\partial \mathbf{u}} = -2 \int_{\Omega} [\mathcal{D}(\mathbf{x}-\mathbf{u}) \Pi_s] \frac{\partial \Pi_s}{\partial \mathbf{x}} d\mathbf{x} = -2 \int_{\Omega} [\mathcal{D}(\mathbf{x}) \Pi_{s(\mathbf{x}+\mathbf{u})}] \frac{\partial \Pi_{s(\mathbf{x}+\mathbf{u})}}{\partial \mathbf{x}} d\mathbf{x}. \quad (7)$$

In the final step of Equation 7, we have substituted  $\mathcal{D}(\mathbf{x}-\mathbf{u})$  by  $\mathcal{D}(\mathbf{x})$  to keep the target shape unchanged during registration. Note that, in the chamfer-matching energy functional in (4), we could also use the  $\mathbf{L}^1$  norm instead of the squared-sum (i.e.,  $\mathbf{L}^2$  norm). However, our experiments showed that the  $\mathbf{L}^1$  norm is more sensitive to local minima, and leads to slower minimization convergence. This observation echoes a similar finding in classic chamfer matching [2].

Given the above chamfer-matching energy, different regularizers and deformation representations can be used for shape registration. In fact, the second-order regularizer of Equation 3 will still be valid when combined with our data term. Alternatively, the B-Spline representation in [4] can also be used. However, non-parametric estimation may not handle some large deformations [4], while spline-based models are limited by the need to explicitly maintain a regular control-point grid (mesh) and connections. Next, we address some of these issues by adopting a meshless representation that approximates the shape's deformation field by blending together local polynomial models using partition-of-unity.

### 3 Meshless deformation model

A limitation of B-spline models is their reliance on an explicit-connected control-point grid (i.e., mesh). Inspired by recent developments in computer graphics [9] and mechanical engineering [10], on building shape functions of arbitrary topology from scattered sample points, we propose a meshless deformation model for shape registration. Although there are meshless shape-deformation models based on thin-plate splines and radial basis functions (RBFs) [1], they are less accurate than polynomial-based representations, as radial basis functions cannot exactly represent polynomial deformations (lack of reproducibility) [10]. In our method, local deformation fields are modeled around scattered nodes (particles) as polynomials, and then blended together into a global deformation field using partition-of-unity. In the following subsections, we first introduce the local deformation model, and then explain how to blend them into a global model.

### 3.1 The node's influence domain

We commence by modeling shape deformation around scattered nodes using polynomial approximation. These nodes can be placed along the shape's contour. As polynomials lack compact support, the approximation is restricted to the node's proximity, a region called the node's *influence domain*. The influence domain also serves to limit the interaction range between neighboring nodes. Let us define the influence domain  $M$  around a node  $p$  as a disk of radius  $r_p$  (ball in 3-D<sup>1</sup>).  $M$  can be modeled by a weighting function  $w_p(\mathbf{x})$  with local support. Various types of weighting functions exist [10]. We define  $w_p(\mathbf{x})$  as:

$$w_p(\mathbf{x}) = \begin{cases} \alpha_p \exp\left(-\kappa \frac{\|\mathbf{p}-\mathbf{x}\|^2}{r_p^2}\right) & , \mathbf{x} \in M \\ 0 & , \mathbf{x} \notin M \end{cases}, \quad (8)$$

where  $\mathbf{p}$  denotes the coordinate vector of node  $p$ ,  $\kappa = \frac{1}{9}$ , and  $\alpha_p \in (0, 1]$  is the node's predefined influence factor in the final global blending. Thus, a node  $p$  is defined by three parameters  $(\mathbf{p}, r_p, \alpha_p)$ , i.e., its spatial position, the radius (scale) of its influence domain, and its influence factor. Note that while the weighting function in (8) is a radial function, its usage is different from previous RBF models such as thin-plate splines [1]. Here, RBFs are used for blending the local polynomial models, instead of directly representing the shape deformation.

### 3.2 Local approximation model around a node

The local deformation field  $\mathbf{u}^p = (u, v)$  around node  $p$  can be expressed as a linear combination of monomials  $x^s y^t$  as follows:

$$u(\mathbf{x}) = \sum_{s,t=0}^{s,t=m} a_{s,t} x^s y^t \quad \text{and} \quad v(\mathbf{x}) = \sum_{s,t=0}^{s,t=m} b_{s,t} x^s y^t, \quad (9)$$

In other words, the local deformation field  $\mathbf{u}_p(\mathbf{x}) = [u(\mathbf{x}), v(\mathbf{x})]^\top$  is represented as a linear combination of monomial basis functions  $\phi^\top(\mathbf{x}) = [1, x, y, xy, x^2, y^2, \dots, x^m y^m]$  with coefficient vector  $\mathbf{d}_p = [a_{0,0}, b_{0,0}, \dots, a_{m,m}, b_{m,m}]^\top$ . The sequence of monomials in  $\phi$  is arranged in a Pascal-triangle manner [10].

### 3.3 Blending local models into a global deformation field

Once the local deformation models are at hand, the deformation at a point  $\mathbf{x}$  is obtained by blending local fields of nodes around  $\mathbf{x}$ , that contain  $\mathbf{x}$  in their influence domains. These nodes are called the *support domain* [10] of  $\mathbf{x}$ , denoted by  $N_{\mathbf{x}} = \{p \mid \mathbf{x} \in M\}$ . The blended global-deformation field is given by:

$$\mathbf{u}(\mathbf{x}) = \sum_{p \in N_{\mathbf{x}}} r_p(\mathbf{x}) \mathbf{u}_p(\mathbf{x}), \quad \text{with} \quad r_p(\mathbf{x}) = \frac{w_p(\mathbf{x})}{\sum_{p' \in N_{\mathbf{x}}} w_{p'}(\mathbf{x})}. \quad (10)$$

<sup>1</sup> A 3-D extension is straightforward.

Here,  $r_p(\mathbf{x})$  ensures the partition-of-unity (PU), i.e., nodes' contributions at  $\mathbf{x}$  must add to one. This blending scheme is equivalent to the Arsigny's polyaffine model [11], and Makram-Ebeid's meshless model [7]. Next, we introduce a novel regularizer to penalize undesired fluctuations in the estimated deformation field.

### 3.4 Consistency enforcement

We have shown that the global deformation can be obtained by blending local deformation fields using Equation 10. In spline-based methods [4], estimated deformation fields are consistent across the control points, and regularization is obtained using Sobolev's norm that penalizes the deformation field's spatial variation. In our method, global deformation fluctuations lead to inconsistencies among local deformation fields. As a result, we penalize the local deformation's *spatial inconsistency*, leading to simpler optimization procedures, as well as to a regularizer that is not biased towards the deformation field's lower-order fluctuations, provided that the fluctuation itself is spatially consistent.

Consistency between two local deformation fields,  $\mathbf{u}_p$  and  $\mathbf{u}_q$ , can be measured from parameters  $\mathbf{d}_p$  and  $\mathbf{d}_q$ . However,  $\mathbf{u}_p$  and  $\mathbf{u}_q$  lie on different local coordinate systems, and therefore need to be aligned. Aligning the basis functions  $\phi$  by  $\Delta\mathbf{x} = [\delta x, \delta y]$  leads to:

$$\begin{aligned}\phi(\mathbf{x} + \Delta\mathbf{x}) &= [1, x + \delta x, y + \delta y, (x + \delta x)(y + \delta y), \dots, (y + \delta y)^m]^\top \\ &= \mathbf{S}^\top(\Delta\mathbf{x})\phi(\mathbf{x}),\end{aligned}\quad (11)$$

where  $\mathbf{S}^\top(\Delta\mathbf{x})$  is the linear *basis-shifting-operator*. Therefore, shifting the local coordinate system leads to shifted polynomial coefficients, and the local deformation consistency between two nodes  $p$  and  $q$  can be defined as:

$$E_{p,q}^c = [\mathbf{S}'(\mathbf{p} - \mathbf{q})\mathbf{d}_q - \mathbf{d}_p]^\top [\mathbf{S}'(\mathbf{p} - \mathbf{q})\mathbf{d}_q - \mathbf{d}_p]. \quad (12)$$

Here, an equivalent shift operator  $\mathbf{S}'(\mathbf{p} - \mathbf{q})$  is created by duplicating and shifting the elements of the basis-shifting-operator. For  $N$  nodes, the global consistency regularizer is obtained by penalizing the average pairwise inconsistency in (12):

$$E^c = \frac{1}{N} \sum_p \left[ \sum_{q \in N_p} w_q(\|\mathbf{p} - \mathbf{q}\|) E_{p,q}^c \right]. \quad (13)$$

### 3.5 Quasi-Newton registration algorithm

We now combine both the chamfer and consistency energies into the following functional minimization problem:

$$\mathbf{d}_p = \arg \min_{\mathbf{d}_p} [E^d(\mathbf{u}) + \lambda E^c], \quad (14)$$

where parameter  $\lambda$  defines the relative importance of the deformation’s spatial consistency. Minimizing (14) can be efficiently achieved using gradient descent [4, 2]. In this paper, we use a quasi-Newton method [12] for its improved convergence speed. The calculation of the required partial derivatives  $\frac{\partial E^d(\mathbf{u})}{\partial \mathbf{d}_p}$  and  $\frac{\partial E^c}{\partial \mathbf{d}_p}$  is straightforward following Equations 6,7,12, and 13.

Using the derived gradients, we implemented an optimization algorithm based on the Broyden-Fletcher-Goldfarb-Shanno (BFGS) method [12]. At each iteration of the algorithm, the source shape is first warped using the deformation field reconstructed from local field parameters (Equation 10), and then its distance transform  $\Pi_{S(\mathbf{x}+\mathbf{u})}$  is updated. Both the destination shape  $\mathcal{D}$  and its distance transform  $\Pi_{\mathcal{D}}$  remain constant. We experimentally determined the search step’s lower bound to be 0.2, and that helps avoid getting trapped in local minima. Additionally, we handle large shape deformations by adopting the hierarchical multi-scale registration strategy used in [4] (i.e., a coarse-to-fine approach).

## 4 Experiments

We tested our method on the Brown University shape dataset [13], and on a cell morphing sequence. Due to the lack of ground truth for shape registration, we demonstrate the results visually in a similar way as in [4, 3, 1]. For the Brown university dataset, the images were first normalized to  $150 \times 150$  sizes, and the shapes were globally aligned beforehand using the rigid registration method implemented in [5]. Then, an initially regular grid of nodes was adapted to the shapes by removing nodes that do not overlap with the shape contour. This adaptation reduced the execution time for about 80 percent on average. In the hierarchical registration algorithm, the space between nodes was 5 pixels at the finest scale, and the node’s radii were 12.5 pixels, i.e., each node interacted with around 20 neighbors. For all shapes, we selected the regularizer weight  $\lambda = 10$ . Figure 2 shows registration results obtained using our method. As in [1], we selected three different shapes (person<sup>2</sup>, hand, and fish), and quantitatively evaluated the registration results. The average pixel distances after local registration for person, fish, and hand were 0.14, 0.24, and 0.08, respectively. This result was better than the one reported in [1], and indicates that shapes were well aligned by our method. Additionally, for most cases, the maximum pixel distance was around 3 pixels showing that registration quality was consistent along contours.

Our method was able to register shapes undergoing large deformation (e.g., bending arm in the person’s sequence). The method also appears to be quite robust to partial occlusion. Figure 3 shows two examples of aligning occluded shapes. Due to severe occlusion, the shapes’ distance transforms (Figure 3(b) and Figure 3(c)) were so distorted that the method in [4] would fail without a proper proximity function (Figure 3(e)). Using only distance values at the shape’s boundary, our method was less sensitive to this distortion (Figure 3(d)).

In the case of the cell-morphing sequence, we manually initialized nodes along the cell’s contour with roughly equal intervals, and the radii of the nodes were

<sup>2</sup> Named dude in the original dataset.

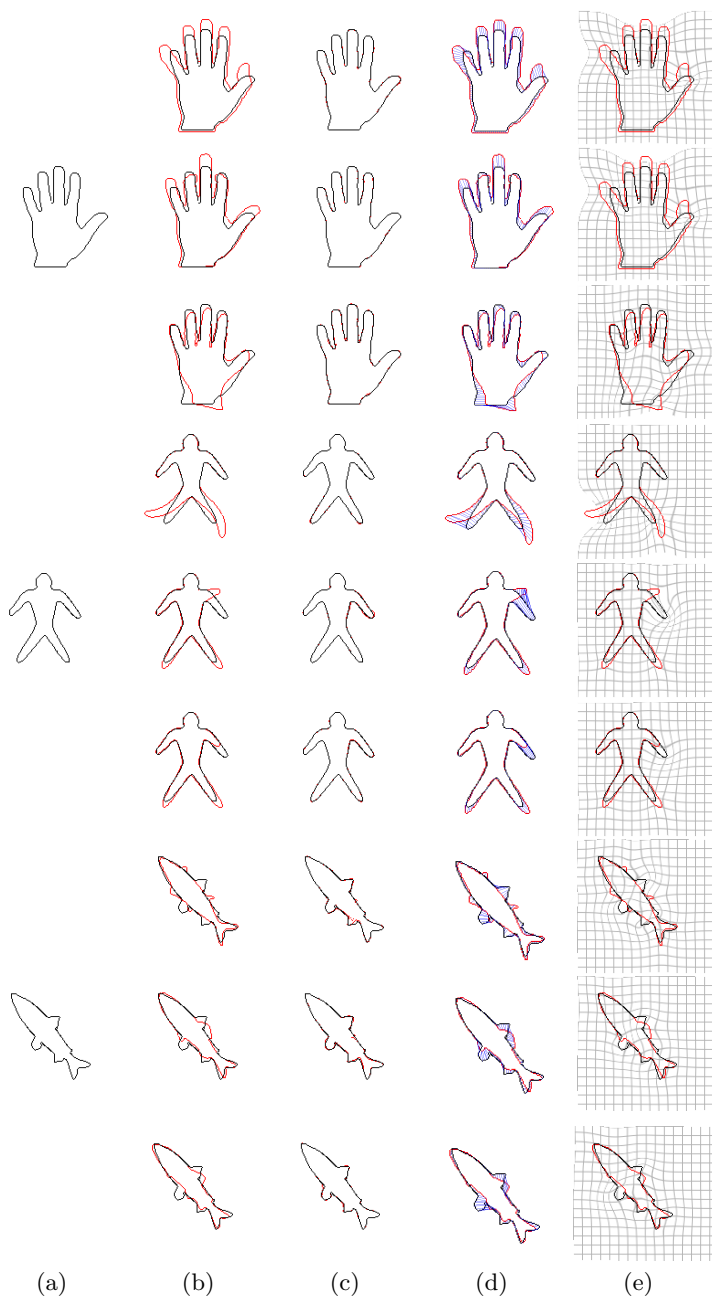


**Fig. 2.** Brown university shape dataset. (a) Target images. (b) Overlaid target (in black) and source images (in red) before registration. (c) After registration. (d) Correspondence between target and source images. (e) Deformation fields as distorted grids.

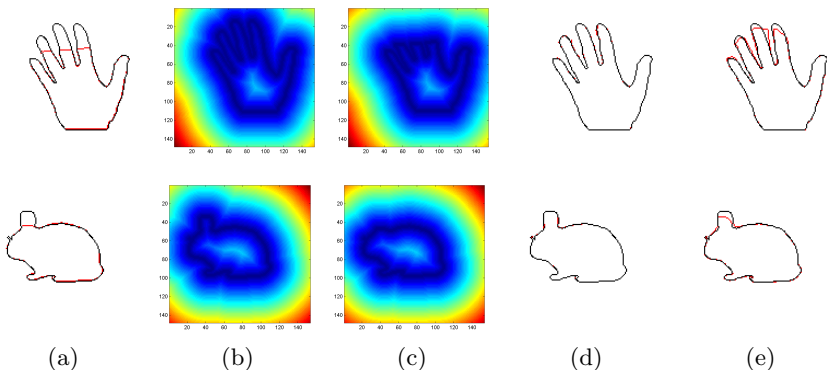


**Fig. 3.** Registration under partial occlusion. (a) Overlaid target and source images. (b) and (c): Distance transforms of target and source images. (d) Our method handles occlusions well as the registration error is only defined along shape contours. (e) The method in [4] would fail to align shape contours without a suitable proximity function.

chosen such that each node had approximately two neighbors. Figure 4(d) shows the distribution of nodes. Here, the node’s positions are indicated as blue crosses, and their radii by circles. This way, the computation cost was significantly reduced. In Figure 4, we show three frames of the cell sequence, and our registration results. The cell’s deformation consisted of its contour bending inwards in the middle. The living cell’s surface exhibited random Brownian motion, with many spurious points, but our method was still able to register their boundaries.

Despite promising results, our method still encounters problems in registering shapes that have large curvatures, and undergo high-degree deformation, causing local minima in the registration error. We believe that this problem can be addressed by adopting global-optimization algorithms such as simulated annealing [12], or by including statistical priors [6].

## 5 Conclusions

A meshless nonrigid shape-registration algorithm was presented. The registration functional is a variational extension of the classic chamfer-matching energy. As in chamfer matching, distance transforms provide registration-error gradients, facilitating efficient registration. Also, we modeled shape deformation using a meshless parametric representation. This model does not rely on a regular control-point grid, and can be adapted to arbitrary shapes. Thus, registration can be focused around the shape contours, greatly improving computational efficiency. We tested the proposed method by registering a number of synthetic shapes, and a deforming cell sequence. Future work includes a 3-D extension of the method, the handling of topological changes, and extensive comparison with state-of-the-art shape registration methods.

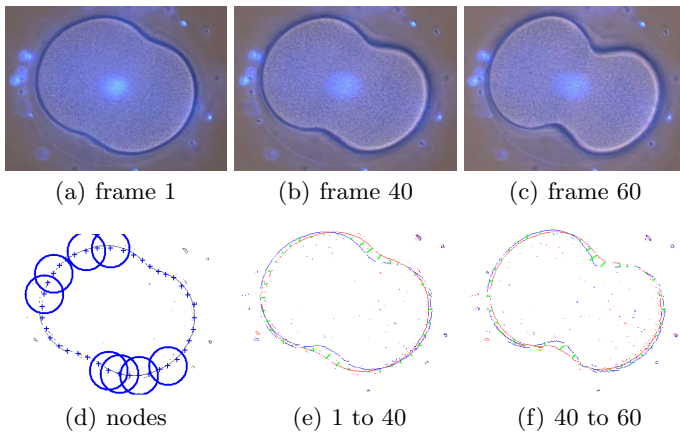


**Fig. 4.** Cell-morphing sequence. (a-c) Frames of a cell morphing sequence. (d) Sample nodes and corresponding influence regions. Nodes are placed along the contour. (e) and (f) Deformation vectors (green arrows).

## References

1. Chen, H., Bhanu, B.: Global-to-local non-rigid shape registration. In: ICPR, Washington, DC, USA, IEEE Computer Society (2006) 57–60
2. Borgefors, G.: Hierarchical chamfer matching: A parametric edge matching algorithm. *IEEE Trans. on Patt. Anal. and Mach. Intell.* **10** (1988) 849–865
3. Paragios, N., Rousson, M., Ramesh, V.: Non-rigid registration using distance functions. *Comp. Vision and Image Underst.* **89** (2003) 142–165
4. Huang, X., Paragios, N., Metaxas, D.: Shape registration in implicit spaces using information theory and free form deformations. *IEEE Trans. on Patt. Anal. and Mach. Intell.* **28** (2006) 1303
5. Kroon, D.J., Slump, C.H.: MRI modality transformation in demon registration. In: ISBI, Piscataway, NJ, USA, IEEE (2009) 963–966
6. Rousson, M., Paragios, N.: Prior knowledge, level set representations & visual grouping. *Int. J. Comput. Vision* **76** (2008) 231–243
7. Makram-Ebeid, S., Somphone, O.: Non-rigid image registration using a hierarchical partition of unity finite element method. *ICCV* **510** (2009) 7
8. Thayananthan, A., Stenger, B., Torr, P., Cipolla, R.: Shape context and chamfer matching in cluttered scenes. In: CVPR, Volume 1. (2003)
9. Ohtake, Y., Belyaev, A., Alexa, M., Turk, G., Seidel, H.P.: Multi-level partition of unity implicits. *ACM Trans. Graph.* **22** (2003) 463–470
10. Liu, G.R.: Mesh free methods: moving beyond the finite element method (Second Edition). CRC (2009)
11. Arsigny, V., Fillard, P., Pennec, X., Ayache, N.: Fast and simple calculus on tensors in the Log-Euclidean framework. In: MICCAI, Springer (2005) 115–122
12. Bonnans, J., Lemaréchal, C.: Numerical optimization: theoretical and practical aspects. Springer-Verlag New York Inc (2006)
13. Sharvit, D., Chan, J., Tek, H., Kimia, B.B.: Symmetry-based indexing of image databases. *J. of Vis. Comm. and Image Repres.* **9** (1998) 366–380